Reversible function switching of Ag catalyst in Mg/S battery with chloride-containing electrolyte

Yan Xu[a,d,1], Yuxing Zhao[b,1], Shuyang Zhao[c], Jifang Zhang[b], Jia Li[c], Jinghua Guo[e,*], Yuegang Zhang[a,b,*]

[a] i-Lab, *Suzhou Institute of Nano-Tech and Nano-Bionics, Chinese Academy of Sciences, Suzhou, Jiangsu 215123, China*
[b] *State Key Laboratory of Low-Dimensional Quantum Physics and Department of Physics, Tsinghua University, Beijing 100084, China*
[c] *Laboratory for Computation Materials Engineering, Division of Energy and Environment, Graduate School at Shenzhen, Tsinghua University, Shenzhen 518055, China*
[d] *Department of Materials Science and Engineering, Stanford University, Stanford, CA 94305, USA*
[e] *Advanced Light Source, Lawrence Berkeley National Laboratory, Berkeley, CA 94720, USA*

ARTICLE INFO

Keywords:
Mg/S battery
Ag catalyst
Switchable function of AgCl
In-situ XRD
In-situ XAS

ABSTRACT

Rechargeable Mg/S batteries suffer from fast capacity decay because of the difficult re-oxidation of MgS. To tackle this problem, we used Ag catalyst in Mg/S cells with Cl^- containing electrolyte, and achieved a greatly improved specific capacity of ~1200 mAh•g^{-1} and a long cycling life of 100 cycles. To understand the mechanism behind this improvement, we employed *in-situ* synchrotron radiation X-ray diffraction and *in-situ* X-ray absorption spectroscopy tools to study the reversible phase transitions during charge/discharge cycling. The *in-situ* experiment results revealed that, at deeply charged state, Ag reacted with Cl^- in the electrolyte to form the AgCl interfacial layer which prevented the physical contact of Ag with elemental S and avoided the formation of Ag_2S; at early discharged state, AgCl transformed back to metallic Ag, which guaranteed its catalytic effectiveness for MgS decomposition. This reversible function switching mechanism of Ag catalyst is completely different from that in Mg/S cells using other catalysts or electrolytes.

1. Introduction

Magnesium (Mg) metal is promising for battery anodes [1]. Unlike its counterpart metallic lithium (Li), Mg can be safely used as a metal anode without dendrite formation [2] in most organic electrolytes. Moreover, Mg is earth abundant and more chemically inert element than Li. Batteries with Mg of high volumetric capacity (3832 mAh•cm^{-3}) as anode and sulfur (S) as cathode have great potential to deliver higher energy density than that of the state-of-the-art Li-ion batteries, thus attracting significant attention [3]. Despite these advantages, Mg/S battery is still facing critical problems which have remained making the electrochemical performance far below practical requirements. The main reason for the poor performance is difficult upon charging as revealed the re-oxidation of MgS by *in-situ* X-ray absorption spectroscopy (XAS) [4]. To address this issue, various works such as using TiS_2 [4] or carbon nanofiber [5] to modify the separator and electrolyte additives like yttrium chloride (YCl_3) [6] or lithium bis(trifluoromethanesulfonyl)imide (LiTFSI) [7] have been done. Despite of the fact that these efforts have improved the performance of Mg/S batteries to a certain degree, it's still not comparable to that of Li/S systems.

Since metal catalysts have been widely used in Li/S system to activate Li_2S for achieving high S utilization, it is reasonable to hypothesize that a metal catalyst could also help the Mg/S chemistry [8], though the reaction mechanism could be quite different. In this work, we firstly assessed the MgS decomposition abilities on metallic Ag by theoretical calculations. We then fabricated a Mg/S@Ag cell with a Cl^- containing electrolyte, and achieved a high discharging capacity of 1000 mAh•g^{-1} after 100 cycles. *In-situ* synchrotron radiation X-ray diffraction (SR-XRD) and *in-situ* XAS measurements were conducted to study the charge/discharge reaction mechanism of the Mg/S@Ag battery. We found its cycling process was accompanied by reversible formation and dissolution of AgCl layer on the Ag surface in Cl^- containing electrolyte. The reversible conversion between Ag at the early charging stage providing efficient catalysis on MgS decomposition and AgCl at the late charging stage providing cathode protection for high S utilization during cycling was the main reason rather than the formation of Ag_2S active material. Our Mg/S battery takes a stride further as a promising energy storage system beyond Li-ion batteries.

* Corresponding author.
E-mail address: yuegang.zhang@tsinghua.edu.cn (Y. Zhang).
[1] Y.X. and Y.Z contributed equally to this work.

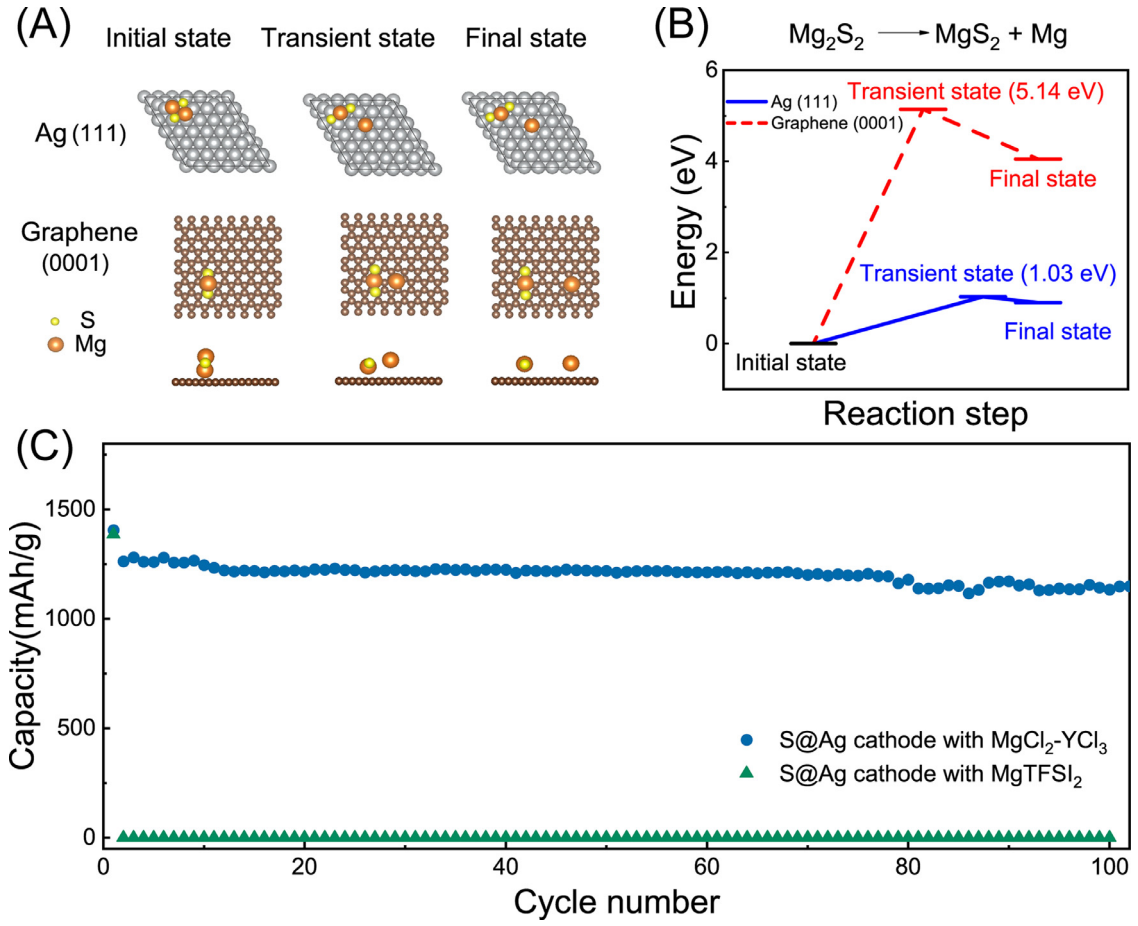

Fig. 1. (A) Computation of energy barriers for MgS decomposition on Ag and graphene surface. From left to right, the MgS decomposition process was described by the evolution of an initial state of a Mg_2S_2 cluster into a transient state until its breakage and forming a final state of a separated MgS_2 cluster and a Mg atom on the Ag (111) and graphene (0001) planes; (B) DFT-calculated energy barriers for MgS decomposition on Ag (blue solid line) and graphene (red dash line) surfaces; (C) cycling performances of Mg/S@Ag cells in Cl^- containing (blue dots) and Cl^- free (green triangle) electrolytes.

2. Results and discussion

Energy barriers for MgS decomposition on graphene and Ag surfaces were calculated using density functional theory (DFT) method. Here, the main MgS decomposition process was described by the evolution of an initial state of a Mg_2S_2 cluster into a transient state where a Mg-S bond was stretched to its maximum until its breakage and formation of a final state of a separated MgS_2 cluster and a Mg atom (Fig. 1A). As shown in Fig. 1B, the MgS decomposition energy barrier on the surface of Ag was 1.03 eV, which was much lower than that on graphene (5.14 eV). A S@Ag cathode was fabricated by a solution-based method which was described in detail in Experimental Section. Scanning electron microscopy (SEM) image in Fig. S1A showed that the pristine Ag substrate was neat and flat. Fig. S1B showed the flake-like morphology of the initial cathode surface after S loading onto Ag substrate. In the X-ray diffraction (XRD) pattern of the initial S@Ag cathode (denoted as "*i*-Ag_2S" in order to distinguish it from any Ag_2S phase possible formed during subsequent electrochemical cycling), major peaks were indexed to Ag_2S (Fig. S1C), indicating that Ag readily reacted with S to form flake-like "*i*-Ag_2S" *via* the solution-based S loading process. The as-prepared S@Ag cathode was paired with a metallic Mg foil and a Cl^- containing $MgCl_2$-YCl_3 electrolyte [4] to assemble a Mg/S@Ag cell for electrochemical measurements. A Cl^- free version cell was also made by using bistrifluoromethanesulfonimide magnesium ($Mg(TFSI)_2$) as electrolyte. The cycling test results in Fig. 1C showed S@Ag cathode in Cl^- containing electrolyte delivered a stable capacity of 1000 mAh•g^{-1} over 100 cycles. Fig. S2 depicted the discharge and charge voltage profile of the Mg/S@Ag cell at 13th cycle. It showed a long discharge plateau above 1.11 V corresponding to the transition reduction process from long-chain polysulfides (MgS_x, $4< x \leq 8$) to short chain polysulfides and a relatively sharp potential drop starting from around 0.94 V which could be ascribed to further reduction of short chain polysulfides to Mg_2S or Mg_2S_2 (Fig. S2). For the Mg/S@Ag cell using Cl^- free electrolyte, however, the capacity quickly decayed from ~1000 mAh•g^{-1} to nearly 0 mAh•g^{-1} within only 2 cycles. The dramatically different results in Fig. 1C provided strong evidence that the combination of Ag catalyst and Cl^- containing electrolyte was the key reason for the highly improved reversibility of the Mg/S cell. A comparison with related works [6–7,9] was summarized in Fig. S3. Our Mg/S@Ag cell using Cl^- containing electrolyte showed the highest reversible discharge capacity and reasonable cycling life.

To gain a deeper insight into the mechanism behind the good performance, *in-situ* SR-XRD was carried out to study the species evolution of S@Ag cathode in the first two cycles (Fig. 2). During the initial activation process (Fig. 2A and B), the intensity of XRD peaks from the "*i*-Ag_2S" starting material decreased significantly, while the peaks at 23.7°, 27.4°, and 39.2° emerged. The emerged peaks corresponded to Ag (111), Ag (200) and Ag (220) planes, respectively, indicating the decomposition of "*i*-Ag_2S" changed into metallic Ag in the S@Ag cathode. Transmission electron spectroscopy (TEM) and energy dispersive X-ray spectroscopy (EDX) were conducted on the initially-discharged S@Ag cathode after the activation process. As shown in Fig. S4, the Mg

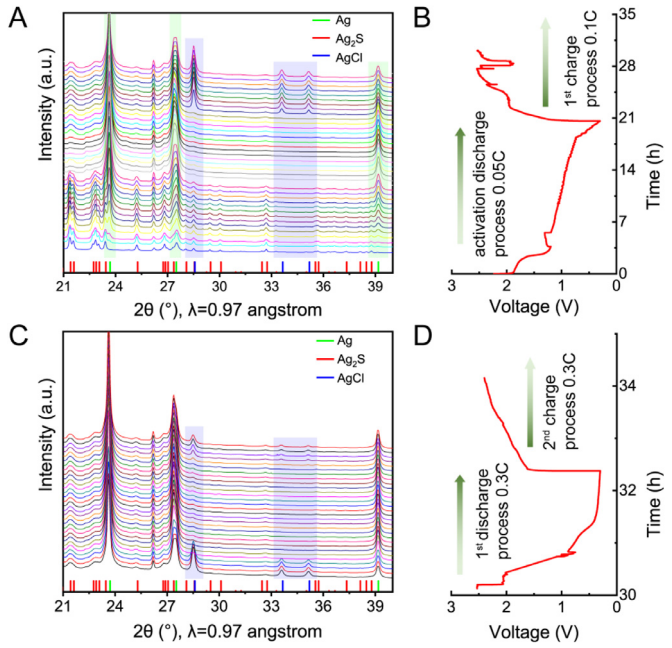

Fig. 2. *In-situ* SR-XRD patterns collected during the (A) activation discharge process and the 1st charge process; (C) the 1st discharge process and the 2nd charge process in a Mg/S@Ag cell. The corresponding chronoperometry profiles collected during the (B) activation process and the 1st charge process and (D) the 1st discharge process and the 2nd charge process in the Mg/S@Ag cell.

and S elements were uniformly distributed on Ag particles, indicating the excellent contact between MgS and Ag. We found that this "*i*-Ag_2S" decomposition process happened only at the initial activation process. After this activation process, Ag_2S peak intensities didn't increase during the subsequent charge process. Instead, we observed emerging peaks of AgCl (220), AgCl (311) and AgCl (222) planes in the 1st charge stage (>2.1 V, see Fig. 2A and B). These AgCl peaks disappeared, gradually, in the subsequent 1st discharge process (Fig. 2C and D).

The coexistence of S and Ag would normally lead to the formation of Ag_2S. However, it was not the case in our Mg/S cell. Further examination of the *in-situ* SR-XRD results in Fig. 2C showed that the AgCl peaks disappeared soon after the 1st discharge started, but emerged again in the late stage of the 2nd charge process. We propose that the reversible formation of AgCl at the deeply charged states during electrochemical cycling would effectively protect S from reduction and prevent the conversion of Ag into Ag_2S (see Fig. S5), and thus the elemental S could be utilized as active materials in subsequent discharge steps, while the catalytic activity of metallic Ag could be maintained for MgS conversion in the next charge.

The formation of AgCl was further confirmed by CV curves of Mg/S@Ag cells using Cl^- containing electrolyte (Fig. S6). The higher potential peak positioned at 1.9 V could be ascribed to the reduction peak of AgCl [10], which was consistent with the XRD results that the peak of AgCl disappeared at the early stage of the discharge process. In order to verify the reduction potential of AgCl, a Mg/AgCl cell was assembled and tested in the same electrolyte as the Mg/S@Ag cell. The voltage profile of Mg/AgCl cell was shown in Fig. S7. The plateau above 1.7 V can be ascribed to the reduction of AgCl. This observation was consistent with those CV curves of S@Ag cathode in Cl^- containing electrolyte and the *in-situ* XRD result, thus confirms the existence of AgCl in the Mg/S@Ag cell. It should be mentioned that a small amount of Ag_2S kept unchanged in the overlapped *in-situ* SR-XRD after the activation process, which could be attributed to the "dead" Ag_2S (Figs. 2 and S8).

We recognized that the *in-situ* SR-XRD method had a drawback that it could only identify crystalline phases, but the electrochemically formed S and MgS products were normally not well crystalized [11]. To further reveal the reaction mechanism of S@Ag cathode, S K-edge XAS was applied to detect S chemical state changes in the Mg/S@Ag cell during the activation and the 1st charge process. The peaks at 2,472.2 eV, 2,475.8 eV and 2,479.0 eV in the S K-edge XAS spectra can be ascribed to S^0, S^{2-}, and $TFSI^-$ ion in the electrolyte, respectively. The black XAS spectrum in Fig. 3A belonged to the initial "*i*-Ag_2S" cathode in Cl^- containing electrolyte. During the activation process, the "*i*-Ag_2S" feature peaks disappeared gradually and the MgS peak (2,475.8 eV) appeared gradually, which indicated the transformation of "*i*-Ag_2S" to MgS (Fig. 3A). This result provided important complementary information to the *in-situ* SR-XRD results in Fig. 2A. During the subsequent 1st charge process, the S^0 peak (2,472.2 eV) increased rather than the Ag_2S peaks, and the MgS peak (2,475.8 eV) decreased continuously as charge proceeded (Fig. 3B), indicating that MgS was decomposed into S^0 without formation of Ag_2S. According to the reported method [12], the changes of S^0 and MgS contents during the charge process could be derived from the fitting parameters of spectra as a function of discharge and charge time (Fig. 3C). The rapid transformation from MgS to S^0 at the early charge stage could be attributed to the catalytic function of Ag.

In light of the *in-situ* SR-XRD and *in-situ* XAS results, we proposed a mechanism for redox reactions in the Mg/S@Ag cell using Cl^- containing electrolyte. In the activation process (Fig. S9), "*i*-Ag_2S" irreversibly reacted with Mg^{2+} to produce metallic Ag and MgS (Reaction 1). In the subsequent 1st charge process, metallic Ag acted as a catalyst to facilitate the reduction reaction of MgS (Reaction 2&3 in Fig. 4). This charge process could be divided into two stages: In the early charge stage, metallic Ag directly catalyzed the reduction of its neighboring MgS into MgS_x (Reaction 2); In the late charge stage, MgS_x was further reduced into elemental S, part of Ag was also oxidized and combined with the Cl^- in the electrolyte to form AgCl layer on the surface

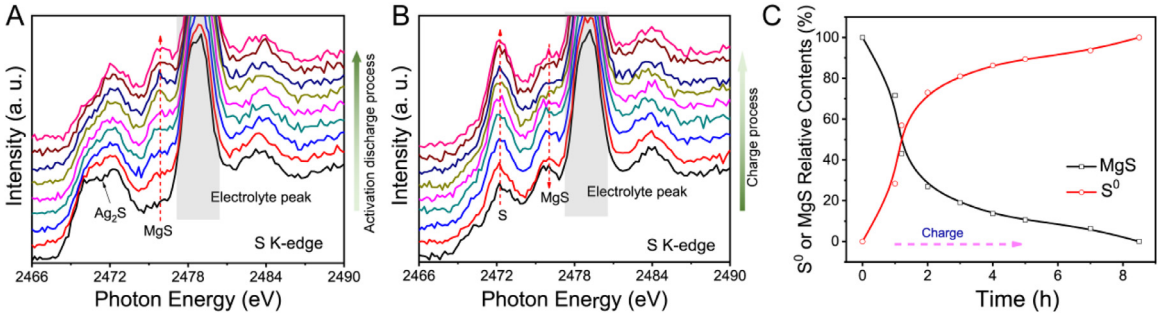

Fig. 3. *In-situ* S K-edge XAS spectra and fitting results from the cathode of the Mg/S@Ag cell. (A) S K-edge XAS spectra collected during the activation process. (B) S K-edge XAS spectra collected during the charge process. (C) Contents of S^0 and MgS calculated from two-phase fitting of the XAS spectra in (B) as a function of time by Athena software. The values of the contents were obtained directly from the fitting parameters of the two-phase fitting spectra.

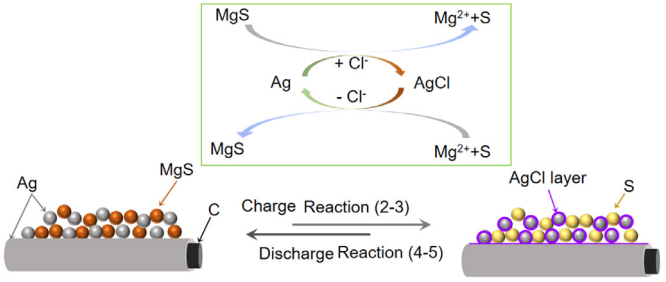

Fig. 4. Schematic illustration of the cathode reaction process in Mg/S@Ag cells.

of metallic Ag (Reaction 3), which separated the metallic Ag from the elemental S and prevented the formation of Ag_2S. The electrochemical reactions in the subsequent discharge process were complete reversal reactions of the charge process, with the decomposition of AgCl back into metallic Ag and the multi-step conversion of elemental S into MgS (Reaction 4&5 in Fig. 4). The following charge/discharge cycles were repetitions of the reversible reactions described in Reaction 2-5. Here, the highly reversible conversion between Ag and AgCl provided switchable functions of AgCl protection for high S utilization and Ag catalysis for effective MgS decomposition, which played a remarkably important role to realize the high performance of Mg/S@Ag cells shown in Fig. 1C.

Activation discharge process:

$$i\text{-}Ag_2S + Mg^{2+} + 2e^- \rightarrow MgS + 2Ag \quad (1)$$

Charge process:

$$xMgS - 2(x-1)e^- \xrightarrow{Ag} MgS_x + (x-1)Mg^{2+} \quad (2)$$

$$MgS_x + (z+1)Ag + zCl^- - (z+2)e^- \rightarrow Mg^{2+} + xS + zAgCl@Ag \quad (3)$$

Discharge process:

$$Mg^{2+} + xS + zAgCl@Ag + (z+2)e^- \rightarrow MgS_x + (z+1)Ag + zCl^- \quad (4)$$

$$MgS_x + (x-1)Mg^{2+} + 2(x-1)e^- \xrightarrow{Ag} xMgS \quad (5)$$

3. Conclusion

3D Ag foam was used as a catalytic current collector that, in combination with a Cl^-containing electrolyte, greatly enhanced the performance (~1000 mAh•g^{-1} over 100 cycles) of Mg/S batteries. *In-situ* SR-XRD and *in-situ* XAS studies revealed that there existed a reversible conversion between Ag and AgCl in the S cathode; and the switchable functions of AgCl protection for high S utilization and Ag catalyzed MgS decomposition are the key for the performance improvement. This finding could lead to better design of S@Ag cathode in future Mg/S batteries.

Declaration of Competing Interest

The authors declare that they have no known competing financial interests or personal relationships that could have appeared to influence the work reported in this paper.

CRediT authorship contribution statement

Yan Xu: Conceptualization, Methodology, Investigation, Writing – original draft. **Yuxing Zhao:** Methodology, Investigation, Writing – original draft. **Shuyang Zhao:** Software. **Jifang Zhang:** Writing – review & editing. **Jia Li:** Software, Resources. **Jinghua Guo:** Resources. **Yuegang Zhang:** Resources, Conceptualization, Writing – review & editing, Supervision.

Acknowledgement

This work was supported by National Key R&D Program of China (2016YFB0100100) and National Natural Science Foundation of China (NSFC U1832218). This work was supported in part by the Beijing Innovation Center for Future Chip (ICFC). The synchrotron X-ray portions of this research were carried out at the Stanford Synchrotron Radiation Light source (SSRL) and Advanced Light Source (ALS). This research used resources of the SSRL, SLAC National Accelerator Laboratory, is supported by the U.S. Department of Energy, Office of Science, Office of Basic Energy Sciences under contract no. DE-AC02-76SF00515. This research used resources of the ALS, which is a DOE Office of Science User Facility under contract no. DE-AC02-05CH11231.

Supplementary materials

Supplementary material associated with this article can be found, in the online version, at doi:10.1016/j.ensm.2021.08.009.

References

[1] (a) D. Aurbach, Z. Lu, A. Schechter, Y. Gofer, H. Gizbar, R. Turgeman, Y. Cohen, M. Moshkovich, E. Levi, Nature 407 (2000) 724–727; b)J.-M. Tarascon, M. Armand, in Materials for Sustainable Energy, 171–179; (c) D. Aurbach, I. Weissman, Y. Gofer, E. Levi, Chem. Rec. 3 (2003) 61–73; (d) H.D. Yoo, Y. Liang, H. Dong, J. Lin, H. Wang, Y. Liu, L. Ma, T. Wu, Y. Li, Q. Ru, Y. Jing, Q. An, W. Zhou, J. Guo, J. Lu, S.T. Pantelides, X. Qian, Y. Yao, Nat. Commun. 8 (2017) 339; (e) X. Cheng, Z. Zhang, Q. Kong, Q. Zhang, T. Wang, S. Dong, L. Gu, X. Wang, J. Ma, P. Han, H.J. Lin, C.T. Chen, G. Cui, Angew. Chem. Int. Ed. Engl. 59 (2020) 11477–11482.
[2] (a) J.W. Choi, D. Aurbach, Nat. Rev. Mater. 1 (2016) 1; (b) S. Chu, A. Majumdar, Nature 488 (2012) 294–303; (c) J. Muldoon, C.B. Bucur, T. Gregory, Chem. Rev. 114 (2014) 11683–11720.
[3] (a) Z. Zhao-Karger, M. Fichtner, MRS Commun. 7 (2017) 770–784; (b) M. Salama, Rosy, R. Attias, R. Yemini, Y. Gofer, D. Aurbach, M. Noked, Acs Energy Lett. 4 (2019) 436–466.
[4] Y. Xu, Y. Ye, S. Zhao, J. Feng, J. Li, H. Chen, A. Yang, F. Shi, L. Jia, Y. Wu, X. Yu, P.A. Glans-Suzuki, Y. Cui, J. Guo, Y. Zhang, Nano Lett. 19 (2019) 2928.
[5] X.W. Yu, A. Manthiram, Acs Energy Lett. 1 (2016) 431.
[6] Y. Xu, G. Zhou, S. Zhao, W. Li, F. Shi, J. Li, J. Feng, Y. Zhao, Y. Wu, J. Guo, Y. Cui, Y. Zhang, Adv. Sci. 6 (2019) 1800981.
[7] T. Gao, M. Noked, A.J. Pearse, E. Gillette, X. Fan, Y. Zhu, C. Luo, L. Suo, M.A. Schroeder, K. Xu, S.B. Lee, G.W. Rubloff, C. Wang, J. Am. Chem. Soc. 137 (2015) 12388.
[8] (a) J. Wang, L. Jia, J. Zhong, Q. Xiao, C. Wang, K. Zang, H. Liu, H. Zheng, J. Luo, J. Yang, H. Fan, W. Duan, Y. Wu, H. Lin, Y. Zhang, Energy Storage Mater. 18 (2019) 246–252; (b) J.L. Wu, J.M. Chen, Y. Huang, K. Feng, J. Deng, W. Huang, Y.L. Wu, J. Zhong, Y.G. Li, Sci. Bull. 64 (2019) 1875–1880; (c) J. Xie, B.Q. Li, H.J. Peng, Y.W. Song, M. Zhao, X. Chen, Q. Zhang, J.Q. Huang, Adv. Mater. 31 (2019) e1903813.
[9] (a) T. Gao, S. Hou, F. Wang, Z. Ma, X. Li, K. Xu, C. Wang, Angew. Chem. Int. Ed. Engl. 56 (2017) 13526–13530; (b) X. Zhou, J. Tian, J. Hu, C. Li, Adv. Mater. 30 (2018) 1704166; (c) L.Q. Zeng, N. Wang, J. Yang, J.L. Wang, Y.L. Nuli, J. Electrochem. Soc. 164 (2017) A2504–A2512; (d) A.B. Du, Z.H. Zhang, H.T. Qu, Z.L. Cui, L.X. Qiao, L.L. Wang, J.C. Chai, T. Lu, S.M. Dong, T.T. Dong, H.M. Xu, X.H. Zhou, G.L. Cui, Energy Environ. Sci. 10 (2017) 2616–2625.
[10] (a) X. Li, Y. Zhang, J. Shen, S.-a. Cao, T. Li, F. Xu, Energy Technol. 7 (2019) 1900454; (b) Y. Zhang, X. Li, J. Shen, Z. Chen, S.A. Cao, T. Li, F. Xu, Dalton Trans. 48 (2019) 14390–14397.
[11] A. Robba, A. Vizintin, J. Bitenc, G. Mali, I. Arcon, M. Kavcic, M. Zitnik, K. Bucar, G. Aquilanti, C. Martineau-Corcos, A. Randon-Vitanova, R. Dominko, Chem. Mater. 29 (2017) 9555.
[12] L. Zhang, D. Sun, J. Feng, E.J. Cairns, J. Guo, Nano Lett. 17 (2017) 5084.